# Design and Dynamics of Flying Height Control Slider With Piezoelectric Nanoactuator in Hard Disk Drives

**Jia-Yang Juang**
e-mail: jiayang@me.berkeley.edu

**David B. Bogy**

Department of Mechanical Engineering,
Computer Mechanics Laboratory,
University of California at Berkeley,
Berkeley, CA 94720

**C. Singh Bhatia**
Hitachi GST,
5600 Cottle Road,
San Jose, CA 95193

*To achieve the areal density goal in hard disk drives of* 1 Tbit/in.$^2$ *the minimum physical spacing or flying height (FH) between the read/write element and disk must be reduced to* $\sim$2 nm. *A brief review of several FH adjustment schemes is first presented and discussed. Previous research showed that the actuation efficiency (defined as the ratio of the FH reduction to the stroke) was low due to the significant air bearing coupling. In this paper, an air bearing surface design, Slider B, for a FH control slider with a piezoelectric nanoactuator is proposed to achieve virtually 100% efficiency and to increase dynamics stability by minimizing the nanoscale adhesion forces. A numerical study was conducted to investigate both the static and dynamic performances of the Slider B, such as uniformity of gap FH with near-zero roll over the entire disk, ultrahigh roll stiffness and damping, low nanoscale adhesion forces, uniform FH track-seeking motion, dynamic load/unload, and FH modulation. Slider B was found to exhibit an overall enhancement in performance, stability, and reliability in ultrahigh density magnetic recording.*
[DOI: 10.1115/1.2401208]

*Keywords: active slider, air bearing surface (ABS), flying height control, hard disk drives, head-disk interface, piezoelectric nanoactuator*

## 1 Introduction

As the spacing between the slider and the disk decreases in hard disk drives, the linear bit spacing of the magnetic recording can decrease, resulting in a higher areal density. According to the Wallace spacing loss equation the magnetic signal increases exponentially as the distance decreases between the magnetic media and the transducer. The maximum magnetic signal can be obtained at a mechanical spacing of zero, resulting in a contact recording scheme. However, there are tradeoffs between reducing the bouncing vibration and wear in such systems [1]. Another significant concern is the thermal stability of both the media and giant magnetoresonance (GMR) sensors. The read-back signal of GMR sensors can be significantly affected by thermal influences since their electrical resistance is temperature dependent. Continuous high-speed contact generates excessive heat, which undermines the recording performance. Also, the air bearing shear force and friction caused by slider–disk contact may affect the tracking ability of these sliders. The above issues have to be addressed before a reliable contact recording system can be realized.

Instead of contact recording, we consider a flying scheme in which the nominal head-media spacing (HMS) has to be reduced to 5 nm for an areal density of 1 Tbit/in.$^2$. This HMS includes a physical spacing (or gap flying height (FH) of 2.5 nm between the read/write element and the surface of the disk, the protective layers–slider and disk diamond-like-carbon overcoats, and lubricants on the disk. A stable and constant gap FH must also be sustained in the presence of altitude and temperature changes, manufacturing tolerance, and track-seeking motion. Furthermore, slider disk contacts must be avoided during load/unload processes and operational shocks. The dynamic instability caused by FH modulations (FHMs) and nanoscale adhesion forces, such as electrostatic and intermolecular forces, should be minimized. Those challenges make a conventional air bearing surface (ABS) slider an unlikely choice for 1 Tbit/in.$^2$. One potential solution is a FH adjustment or controlled slider that is capable of adjusting its gap FH. Table 1 summarizes the challenges of the head–disk interface (HDI) for ultrahigh density recording and potential solutions provided by a FH control slider. Several approaches have been reported for FH adjustment or control as shown in Table 2 [2–22]. They are categorized into five major principles of actuation with four different actuation mechanisms. The effect of air bearing coupling indicates whether one particular actuation is coupled with the air bearing. Such an effect has to be minimized to increase the actuation efficiency (defined as the ratio of FH reduction to actuation stroke). Khanna et al. [11] in 1991 and then Zhang et al. [12] in 2005 reported a method of FH adjustment by bonding a bulk piezoelectric material on the back side of a slider body. The FH was adjusted by applying a voltage to the piezoelectric material and thereby changing the crown and/or camber of the slider body. The structure of such sliders is simpler and it is relatively easy to fabricate but the fact that the actuation is coupled with the air bearing significantly limits the actuation stroke and efficiency. Instead of piezoelectric materials, Dietzel et al. [13] used a microfabricated thermal actuator to deform the slider body. Besides the disadvantage of air bearing coupling, the power consumption was very high compared to the operating power of an HDD, especially for mobile applications. Another principle of actuation is to apply an electrostatic force in the HDI [18,19] or to change the pattern of air flow by ducts and valves [20]. Besides the disadvantage of air bearing coupling, the former also significantly increases the risk of electrostatic discharge (ESD) across the interface and the latter has difficulty achieving a high resolution FH adjustment. Another approach is to bond a layer of piezoelectric material to one side of the suspension and change the FH by bending the suspension [21,22]. Besides the strong coupling of the actuation and the air bearing, the bandwidth of actuation is limited by that of the suspension dynamics, which is much lower than that of the

Contributed by the Tribology Division of ASME for publication in the JOURNAL OF TRIBOLOGY. Manuscript received March 15, 2006; final manuscript received June 17, 2006. Review conducted by Takahisa Kato.

  

**Table 1 Challenges of ultralow flying sliders and potential solutions provided by a controlled FH slider**

| Challenges | Potential solutions |
|---|---|
| FH drop due to altitudes | FH adjustment (with a pressure sensor) |
| FH drop during seek motions | High roll stiffness and low skew angle sensitivity |
| Manufacturing tolerance ($\sigma$) | FH adjustment |
| Load/unload process | • Retract the read/write element while loading/unloading<br>• High roll stiffness and damping |
| Operational shock | • Retract the read/write element during shocks (with an accelerometer)<br>• High stiffness and damping |
| FHM and nanoscale adhesion forces (such as electrostatic and intermolecular forces) | • Reduce those forces by reducing the area of central trailing pads<br>• FHM suppression by dynamic feedback control (with a feedback of readback signals) |

air bearing. Another concept of actuation is to drive the read/write elements so that they have relative displacement to the slider body. Due to the minute area that the read/write element occupies on the slider air bearing surface, the effect of air bearing coupling could be minimized. Chen et al. [17] designed a micromachined monolithic electrostatic actuator for adjusting FH. However, such an actuator was susceptible to particle contamination due to the complex structure of the multiple parallel plates and the electrostatic attraction force. The concept of adjusting the transducer FH by the thermal expansion of materials was first demonstrated by Meyer et al. [14], in which a resistance heating element (heater) was mounted to the slider body near the read/write element. When a current is applied through the heater a portion of the head protrudes due to the mismatch of the coefficients of thermal expansion of the various materials. Such protrusion reduces the FH. Juang et al. [15] found that even though the protruded area was relatively small, there was still considerable air bearing coupling with the resulting actuation efficiency of only 63%. The authors further designed an ABS for such sliders with much higher actuation efficiency [16], which suggested that the ABS played a key role in reducing the air bearing coupling. Another approach that can potentially exhibit high actuation bandwidth, low power consumption, and less air bearing coupling is to utilize piezoelectrically actuated unimorph cantilever sliders. Yeack-Scranton et al. [9] proposed an active slider for contact recording, where a piezoelectric material was inserted into a channel that ran across the full width of the slider at its top rear. They experimentally demonstrated movement of the read/write element from ~200 nm to contact, but the proposed structure of piezoelectric actuator was difficult to implement in the smaller currently used pico- or femto-sized sliders and the effect of the air bearing was not discussed. Juang et al. [10] numerically and experimentally studied an $Al_2O_3$–TiC slider with a unimorph piezoelectric cantilever. They used a conventional ABS and found that the actuation efficiency was very low due to the highly pressurized central trailing pad. Several papers, such as Kurita et al. [2,3], Tagawa et al. [5], Suzuki et al. [4], and Su et al. [6], have presented active sliders made of silicon with piezoelectric unimorph cantilevers. The slider structure was simpler and could be fabricated by silicon microfabrication technology. An ABS design with less air bearing coupling effect was also proposed, which was achieved by a small central trailing pad. The increase of aerodynamic lift force caused by the bending of the cantilever was minimized such that the flying attitude of the slider body was hardly changed during the head actuation. However, the use of silicon as the slider material makes it difficult to integrate with current fabrication technology. Also, the two slots that defined the cantilever significantly reduced the amplitude of the negative pressure of their subambient ABS sliders and the negative pressure is known to be a key attribute for high performance sliders. Since such sliders have several merit features over other FH control schemes, it is important to study and design an ABS for such sliders with high negative pressure and other required characteristics.

In this paper, we present a novel ABS design for FH control sliders with a piezoelectric unimorph nanoactuator, which can achieve high actuation efficiency (or little air bearing coupling),

**Table 2 Comparison of FH adjustment/control sliders [2–22]**

| Principle of actuation | Actuation mechanism | Air bearing coupling | Authors |
|---|---|---|---|
| Unimorph cantilever | Piezoelectricity | No | Kurita [2,3]; Suzuki [4], Tagawa [5], Su [6], Juang [7,8] |
| | Piezoelectricity | Yes | Yeack-Scranton [9], Juang [10] |
| Change of crown/camber | Piezoelectricity | Yes | Khanna [11], Zhang [12] |
| | Thermal expansion | Yes | Dietzel [13] |
| Relative displacement of read/write elements | Thermal expansion | N/A[a] | Meyer [14] |
| | Thermal expansion | Yes | Juang [15] |
| | Thermal expansion | No | Juang [16] |
| | Electrostatic force | N/A[a] | Chen [17] |
| Forces in HDI | Electrostatic force | Yes | Song [18], Feng [19] |
| | Change of air flow by ducts and valves | Yes | Albrecht [20] |
| Suspension bending | Piezoelectricity | Yes | Good [21], Liu [22] |

[a]Not available.

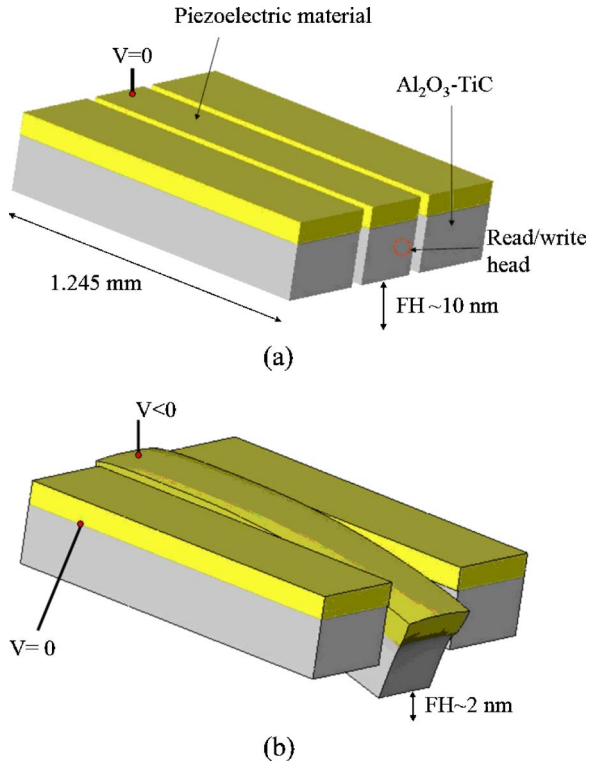


**Fig. 1 Two operational modes of a FH control slider with piezoelectric actuation: (*a*) passive mode; (*b*) active mode**

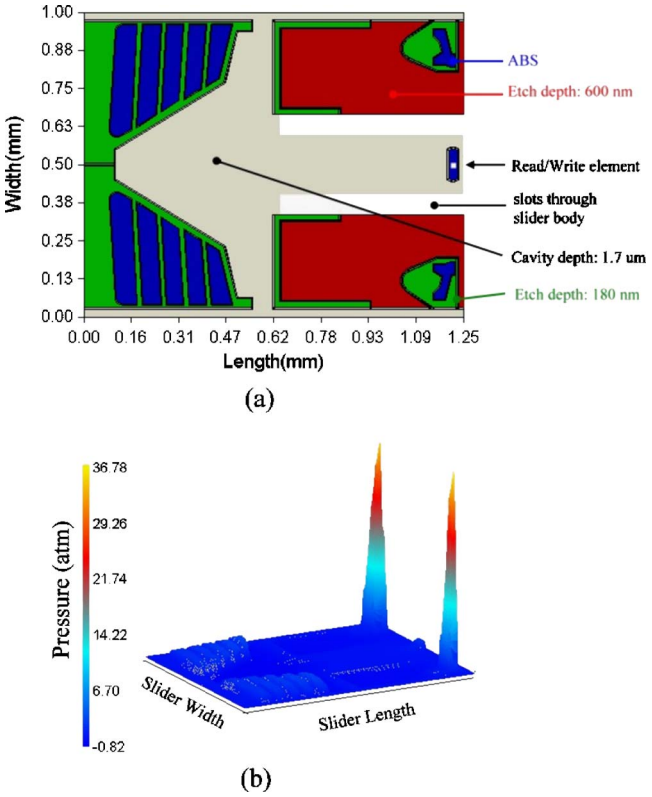


**Fig. 2 (*a*) Air bearing surface design, Slider B; and (*b*) air bearing pressure profile at the MD (radial position 23.88 mm, skew: –2.56 deg). The scale displayed is normalized to ambient pressure: $(p-p_a)/p_a$.**

high negative pressure, high air bearing stiffness, and damping. Numerical studies of the static and dynamic performances, including flying attitude, actuation efficiency, nanoscale adhesion forces, track-seeking motion, dynamic load/unload, and FHM, are carried out and discussed. The results are also compared with conventional ABS designs.

## 2 Design Concept

In order to actively control the gap FH, we consider an active slider with piezoelectric nanoactuator as shown in Fig. 1. The FH is about 10 nm in the off duty cycle (passive mode) and is reduced to ~2 nm during reading and writing (active mode) by applying a voltage to the central piece of piezoelectric material. The actuation stroke is a function of the applied voltage, the air bearing force generated by the central trailing pad, the actuator geometry, and materials [7,8]. Such reduction of FH of several nanometers is expected to permit the increase in the areal density from less than 100 Gbit/in.$^2$ to 1 Tbit/in.$^2$. The proposed ABS design, called Slider B, is illustrated in Fig. 2(*a*). It has four levels of etching steps. The recessed areas with 1.7 $\mu$m and 600 nm etch depths create a subambient pressure zone and a negative pressure distribution (suction force), "pulling" the slider toward the disk surface. The two side trailing pads generate a positive pressure distribution (lift force), "pushing" the slider away from the disk surface (Fig. 2(*b*)). Those negative and positive pressure distributions balance with the applied gram load and together determine the flying attitude, such as FH, pitch and roll, and other important characteristics, including air bearing stiffness and damping. The read/write element is located near the center of the trailing pad of the slider body. The targeted gap FH (without actuation) is 10 nm at a disk velocity of 15,000 rpm. Slider B was designed to achieve high actuation efficiency (low air bearing coupling) and to meet the following requirements: (1) constant FH profile from the inner diameter (ID) to the outer diameter (OD) with skews; (2) high roll stiffness and damping; (3) reduced effect of nanoscale adhesion forces in the HDI; (4) less FH changes during track-seeking motions; (5) better dynamic load/unloadperformance; and (6) comparable FHM. The features of Slider B include the two slots defining the cantilever, the microtrailing pad, the cavity walls enclosing half of the two 600 nm side etch levels, and the stripes on the two leading pads. The slider is primarily supported by the positive force generated by the two side-trailing pads as seen in Fig. 2(*b*). The two slots allow the cantilever to move upward or downward, i.e., to adjust the FH. The reduced area of the microtrailing pad effectively minimizes the air bearing coupling effect and the nanoscale adhesion forces, such as electrostatic and intermolecular forces. The cavity walls hold the negative pressure without it leaking to the slots and hence increase the stiffness. The multiple stripes create pressure gradients and increase the air film damping [23]. A conventional ABS, Slider A, is used for comparison (Fig. 3). Those results are shown and discussed in the following sections.

## 3 Static Analysis

**3.1 Flying Attitude and Actuation Efficiency.** Numerical simulations were performed using the CML static air bearing simulator, which solved the generalized Reynolds equations and determined the steady-state flying attitude, including FH, pitch, and roll. The disk radius/skew range is 17.87 mm/−15.62 deg to 29.89 mm/7.22 deg with a disk velocity of 15,000 rpm, corresponding to linear velocities of 28 m/s and 47 m/s at the ID and the OD, respectively. Positive skew indicates that air flows from the outer leading edge to the inner trailing edge. The simulation conditions and air bearing specifications are summarized in Table 3. In Fig. 4 it is seen that a nearly uniform 10 nm FH is achieved with minimal loss at high altitude (4500 m). The roll angle is less than 3 $\mu$rad over the disk. A relatively high negative (suction) force is also preserved, which is needed to maintain high stiffness

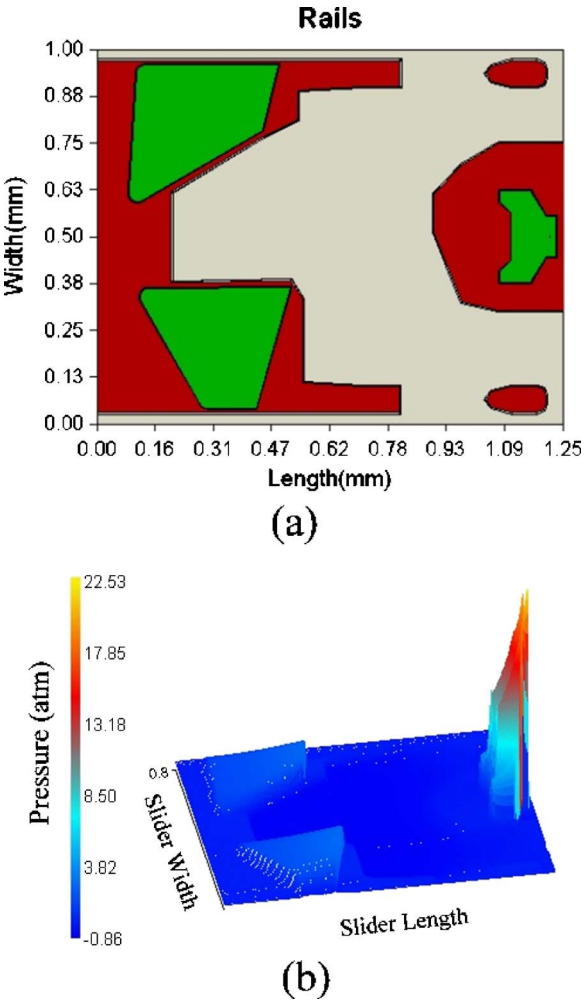


**Fig. 3 (*a*) A conventional pico-slider ABS, Slider A, used for comparison; and (*b*) air bearing pressure profile at radial position 23.88 mm. The scale displayed is normalized to ambient pressure: $(p-p_a)/p_a$.**

and low sensitivity to ambient pressure change.

Figure 5 shows the simulated FH as a function of actuation stroke. Due to the small area of the central trailing pad and the support of the two side trailing pads, the actuation is not coupled with the air bearing pressure and a high actuation efficiency (=FH reduction/stroke) of 98.75% is achieved. It is seen that the reduction of gap FH is virtually proportional to the stroke and the FH of

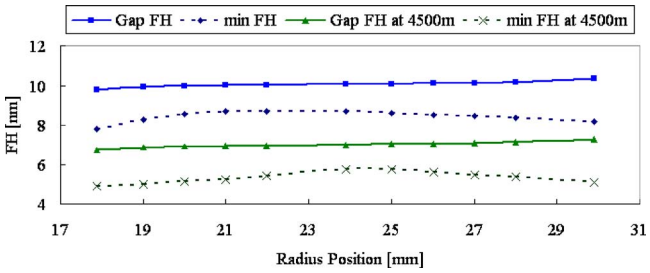


**Fig. 4 Simulation of gap FH and minimum FH profiles of Slider B at sea level, 0 m, and high altitude, 4500 m**

the rest of the slider is nearly unchanged. A small increase of air bearing pressure is observed when the slider has an 8 nm actuation stroke (Fig. 6).

**3.2 Stiffness and Damping of the Air Bearing.** The air bearing stiffness and damping of a particular slider design are primarily determined by the geometry of the air bearing surface. It has been shown that high stiffness and damping are desired for a reliable and stable HDI. Modal analysis and the system identification method were used to calculate the frequency responses and obtain the modal parameters, such as modal stiffness, damping ratios, and nodal lines, of the air bearing slider [23]. Figure 7 shows the frequency responses of Slider B and Slider A. It is seen that Slider A exhibits a typical three-peak curve, corresponding to the first pitch, second pitch, and roll modes. It is noted that Slider B shows only one peak, which clearly indicates that the damping ratios for the other two modes are very large. Comparisons of the modal frequencies, stiffness, and damping ratios with published data in Refs. [24,25] are shown in Fig. 8 and Table 4. Among the four ABS designs, Slider B shows a significant increase of 52%, 506%, and 237% in damping ratios over the second most highly damped ABS II for the first pitch, second pitch, and roll modes, respectively. As listed in Table 4, Slider B exhibits a 694% increase in the roll stiffness over Slider A but it shows a 24% and 28% decrease of the first and second pitch stiffnesses, respectively. It will be demonstrated in Sec. 4 that the dynamical performance of Slider B is greatly enhanced, which is primarily attributed to the significant increase of the roll stiffness and damping.

**3.3 Nanoscale Adhesion Forces.** Nanoscale adhesion forces, such as electrostatic and intermolecular forces, can cause dynamical instability in the HDI of ultralow flying sliders [26]. Even though those forces cannot be completely attenuated, their effect can be reduced by simply decreasing the effective slider area within proximity of the disk. For a FH control slider, this reduction in area is achieved by flying at a higher FH and bending the microsized central trailing pad close to the disk. Numerical simulations were performed to investigate the effect of such forces on

**Table 3 Air bearing specifications and flying attitudes for slider B**

Slider Size (mm): 1.245×1.000×0.300
Crown: 9.3 nm
Camber: −2 nm
Suspension load: 2.0 gf
Disk rpm: 15,000

| Radial position (mm) | 17.87(ID) | 21 | 23.88(MD) | 27 | 29.89(OD) |
|---|---|---|---|---|---|
| Skew (°) | −15.62 | −8.197 | −2.56 | 2.768 | 7.22 |
| Pitch ($\mu$rad) | 103.03 | 107.64 | 108.55 | 107.39 | 105.16 |
| Roll ($\mu$rad) | −2.07 | −0.24 | −0.32 | −1.25 | −2.58 |
| Gap FH (nm) | 9.77 | 10.01 | 10.05 | 10.13 | 10.33 |
| Minimum FH (nm) | 7.81 | 8.69 | 8.70 | 8.45 | 8.18 |
| Negative force (gf) | −2.92 | −3.02 | −3.09 | −3.17 | −3.24 |

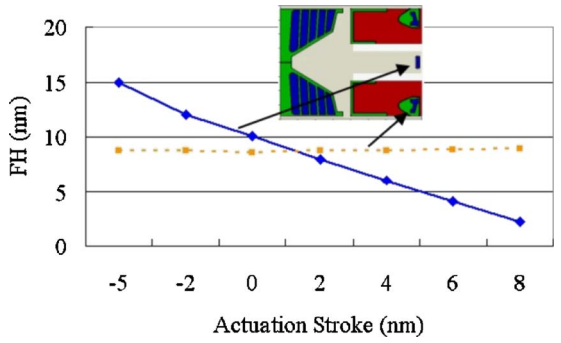


**Fig. 5 Simulated FHs at the read/write transducer and one point on one of the side ABS rails. The radial position is at the MD.**

the flying attitude of Slider B. Figure 9 shows the minimum FH as a function of electrostatic potential between the slider and the disk for three different ABS designs, where the 5 nm minimum FH of Slider B at zero voltage is obtained with a 4 nm actuation stroke. It is seen that the breakdown voltage of Slider B (with 108 $\mu$rad pitch) is 27% and 43% higher than the high-pitch slider (245 $\mu$rad) and low-pitch slider (190 $\mu$rad), respectively. Similarly, in comparing the intermolecular force, Slider B exhibited a 24–28% decrease within the 2–4 nm FH region as shown in Fig. 10.

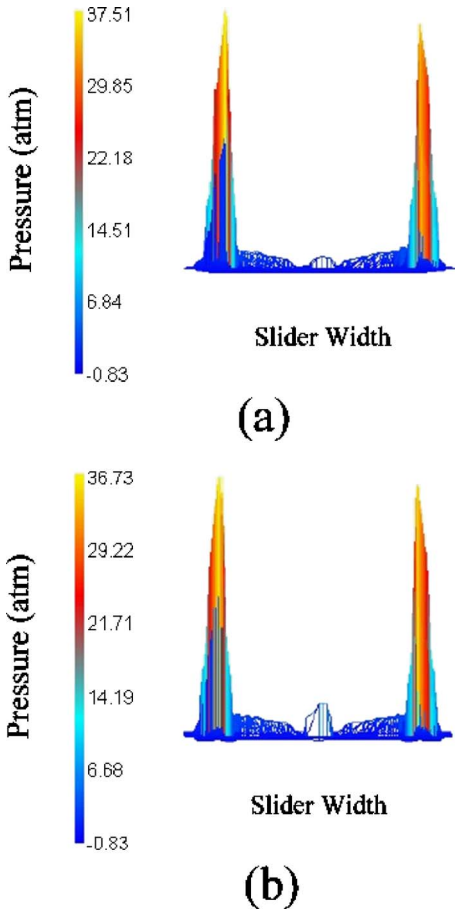


**Fig. 6 Air pressure distributions before (*a*) and after (*b*) a 8 nm actuation stroke**

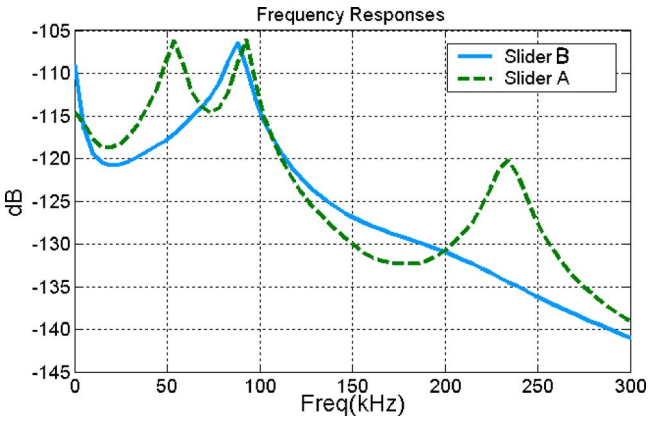


**Fig. 7 Frequency responses of the air bearings of Slider B and Slider A**

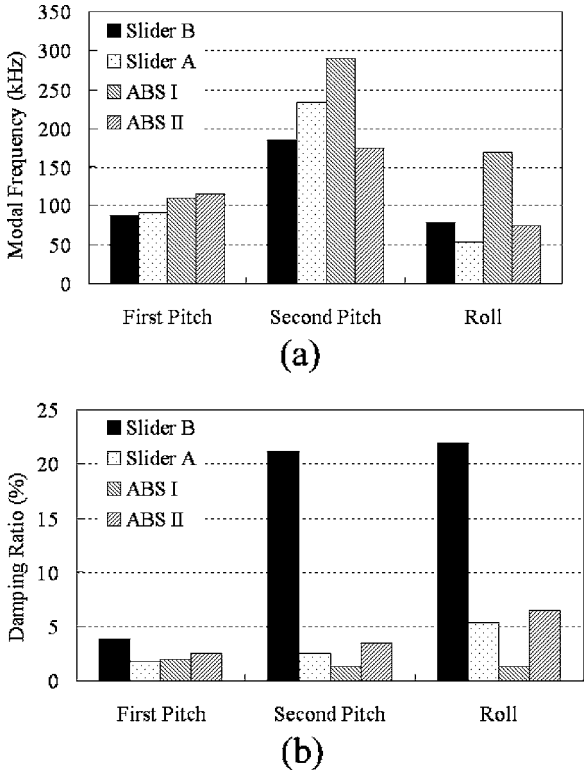


**Fig. 8 Comparison of modal frequencies and damping ratios of various ABS designs. The data of Slider B and Slider A were evaluated at the MD. The data of ABS I and ABS II were obtained from Ref. [24].**

**Table 4 Comparison of air bearing stiffness of various ABS designs. The data of slider B and slider A were evaluated at the MD**

| | Slider B | Slider A | Multilevel cavity [25] | Single-level cavity [25] | ABS I [24] |
|---|---|---|---|---|---|
| Form factor | pico | pico | pico | pico | pico |
| Gap FH (nm) | 10.05 | 10.65 | 10.23 | 10.25 | 4.80 |
| Pitch ($\mu$rad) | 109 | 126 | 230 | 229 | 214 |
| Roll ($\mu$rad) | −0.3 | −1.4 | 0.5 | −0.7 | 0.8 |
| $k_z$ (gf/nm) | 0.182 | 0.239 | 0.164 | 0.090 | 0.178 |
| $k_p$ ($\mu$N m/$\mu$rad) | 0.517 | 0.715 | 0.49 | 0.200 | 0.537 |
| $k_r$ ($\mu$N m/$\mu$rad) | 0.246 | 0.031 | N/A[a] | N/A[a] | 0.059 |
| Negative force (gf) | −3.1 | −4.0 | −3.9 | −2.8 | −3.1 |

[a]Not available.

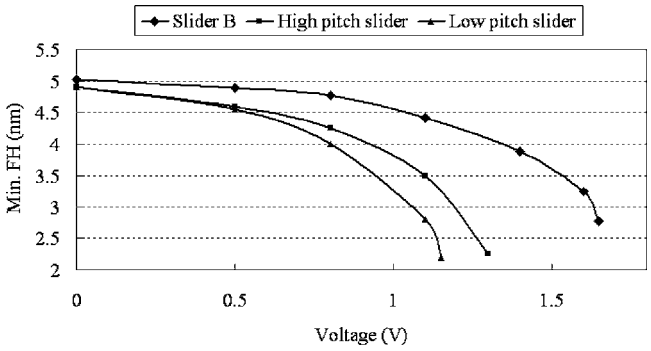


**Fig. 9 The drop of minimum FH caused by the electrostatic potential across the HDI. The actuation stroke of Slider B is 4 nm. The pitch of Slider B is 108 $\mu$rad at zero voltage. The results of the high-pitch slider (245 $\mu$rad) and low-pitch slider (190 $\mu$rad) are from Ref. [26].**

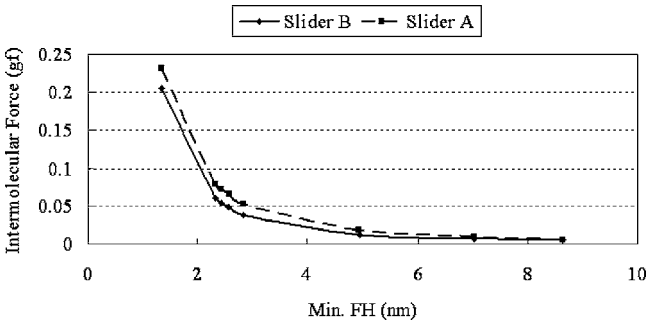


**Fig. 10 Comparison of magnitudes of intermolecular adhesion forces of Slider B and Slider A as a function of minimum FH. The FH of Slider B was reduced by actuating the central trailing pad toward the disk and the obtained flying attitudes (minimum FH, pitch, and roll) were then used to calculate the intermolecular forces of Slider A.**

## 4 Dynamic Analysis

The air bearing film and slider body form a complex coupled nonlinear dynamic system. The CML dynamic air bearing simulator is used to solve the generalized Reynolds equations coupled with the dynamics of the slider body and a lumped parameter suspension, where the suspension is represented by flexure stiff-

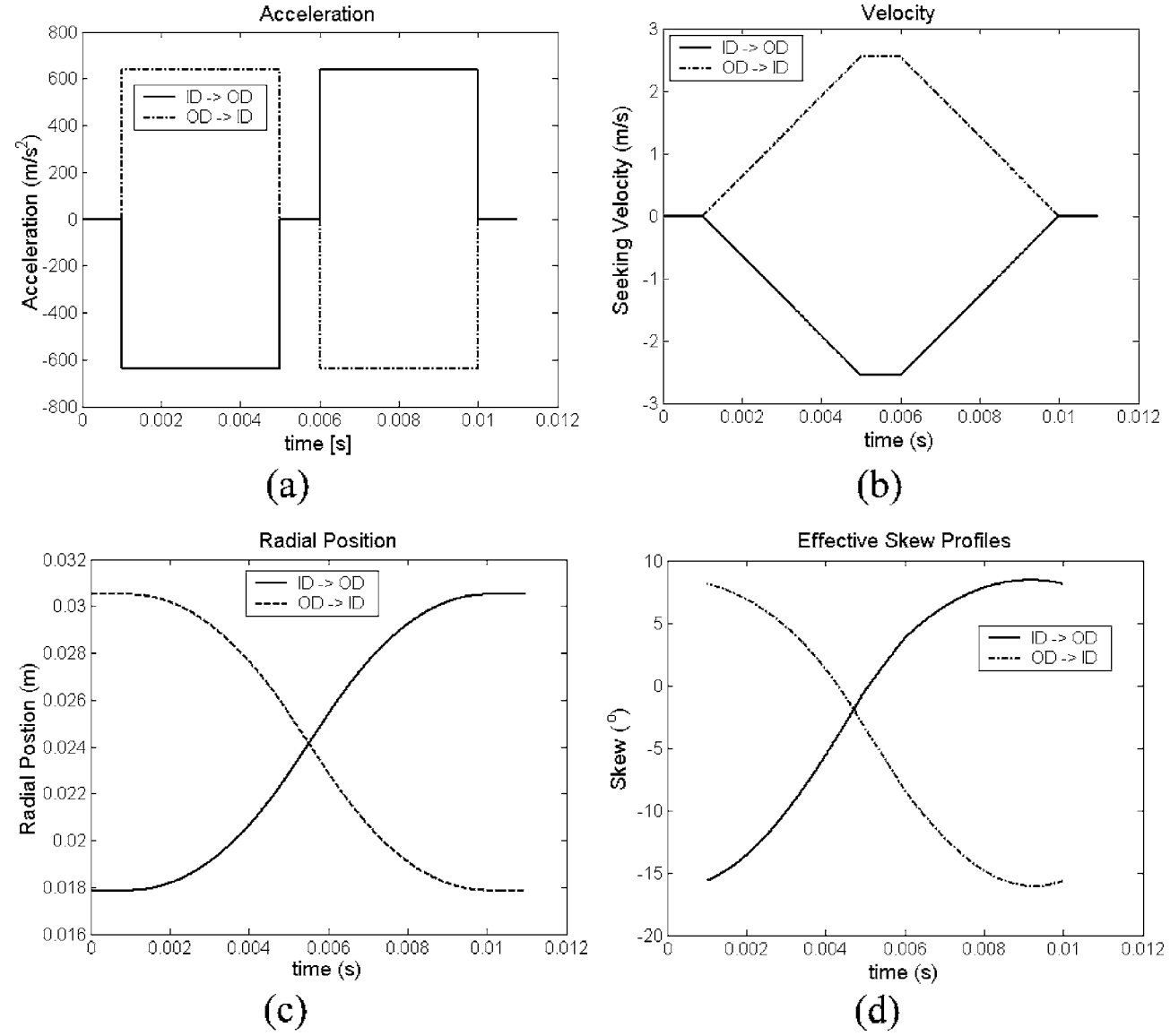


**Fig. 11 Track-seeking profiles. The maximum acceleration is 65 g.**

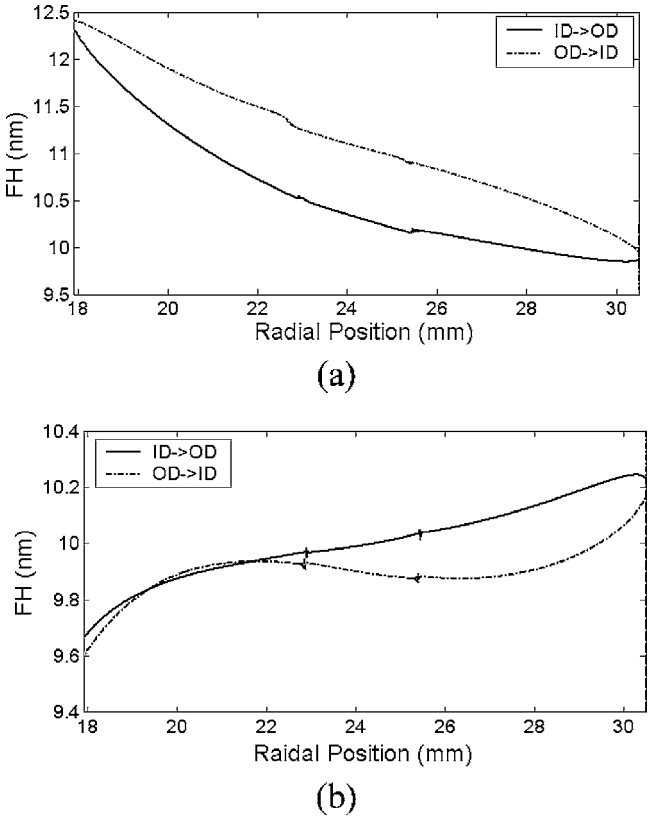


**Fig. 12 Gap FH changes due to the seek motion for (*a*) Slider A (with a maximum difference of ~0.75 nm near the MD); and (*b*) Slider B (with a maximum difference of ~0.2 nm near the OD)**

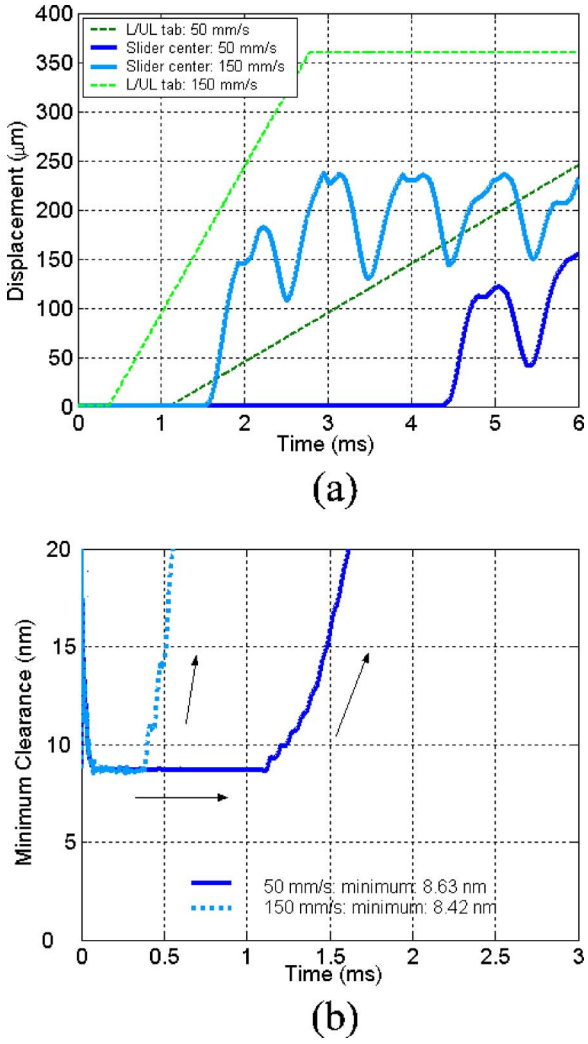


**Fig. 13 Comparison of the displacement and minimum clearance histories during the unloading processes with two unloading velocities, 50 mm/s and 150 mm/s, at the OD (7.22 deg skew) and 15,000 rpm**

ness and damping coefficients. By using the simulator, we can obtain dynamic responses of a slider subject to various dynamic inputs, including the flying characteristics during track-seeking motion and FHM over measured disk morphology. The CML load/unload and shock simulator, developed by Bhargava and Bogy [27], is used to simulate complex dynamic responses of a slider in the load/unload process and under operational shock. This simulator is based on the dynamic simulator and uses more sophisticated finite-element models for the suspension and disk.

**4.1 Flying Characteristics During Track-seeking Motion.** Track seeking is the process for a slider to move from one track to another. During this process, the FH changes as a result of the skew angle and the relative disk velocity, as well as the inertia force due to the slider's acceleration or deceleration in the cross-track direction. Track access time is one of the important hard drive performance indices. Increasing the seek acceleration can reduce the access time. However, it also leads to larger inertial effects and adversely increases FH drops. Figure 11 shows the track-seeking profile used in this study. The maximum acceleration is 65 g and it takes 11 ms for seeking from the ID to the OD or vice versa. The effective skew angle is the angle between the slider's longitudinal direction and the relative disk velocity (or air flow velocity) which is the resultant vector of the disk track linear velocity and the slider's seek velocity. The FH changes of Slider A and Slider B during the seek motion are shown in Fig. 12. It is seen that Slider B exhibits a remarkable flat FH during the entire seek profile with a maximum FH difference of about 0.2 nm near the OD, as compared with the 0.75 nm FH difference of Slider A near the molecular dynamics (MD). Since Slider B has an ultra-high roll stiffness, its sensitivity to the skew angle change is significantly reduced, hence, resulting in a more uniform FH profile.

**4.2 Dynamic Load/Unload Performance.** Dynamic load/unload (L/UL) has been widely used in recent hard disk drives for achieving better shock resistance, lower power consumption, as well as lower wear and debris. Previous research showed that the ABS design significantly affects the L/UL performance [28,29]. The main design objectives of L/UL are no slider–disk contact during the entire L/UL and a smooth and short unloading process. Challenges exist in both the loading and unloading processes. During the loading process, sliders may hit the disk especially at high loading velocities. In the unloading process, the air bearing positive pressure quickly responds to changes in FH and pitch, while the suction force generated by subambient cavities is relatively resistant to change. This results in a net suction force, which in turn causes slider–disk contact. The subambient pressure therefore plays a key role in the L/UL processes. While the likelihood of contact can be decreased or eliminated by reducing the suction force, this force is beneficial to maintain high stiffness and low fly sensitivity. Another potential solution is to use a slider with burnished or rounded corners [30]. However, this additional corner rounding can cause sensitivity of the FH to tolerances associated with the manufacturing process. Another solution is to design an ABS with high roll stiffness so that it can avoid the undesirable roll motion during unloading. It has been shown in the previous section that Slider B has much higher roll stiffness compared to

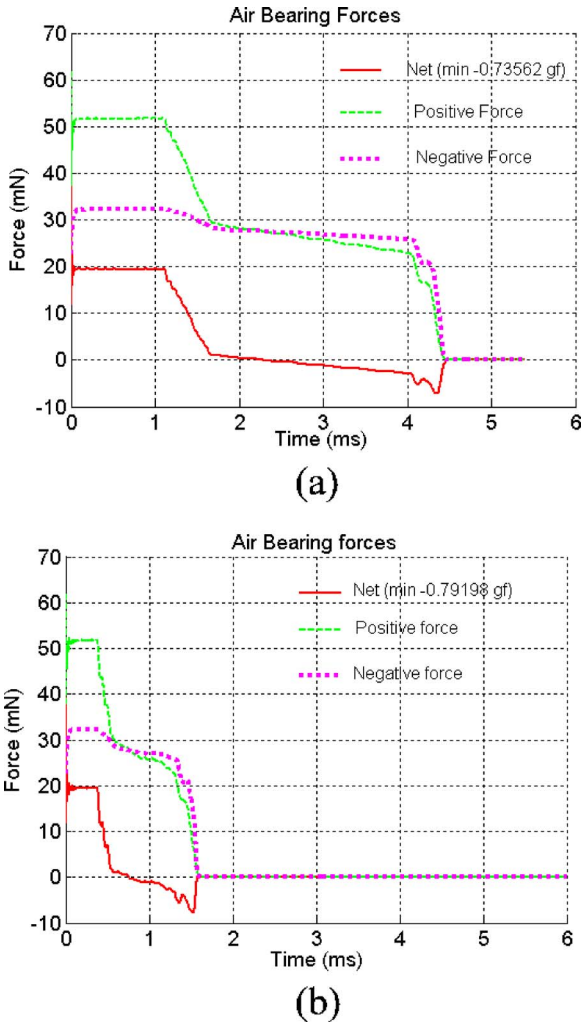


**Fig. 14 Air bearing force histories during unloading processes at the OD: (*a*) unloading velocity: 50 mm/s; and (*b*) 150 mm/s**

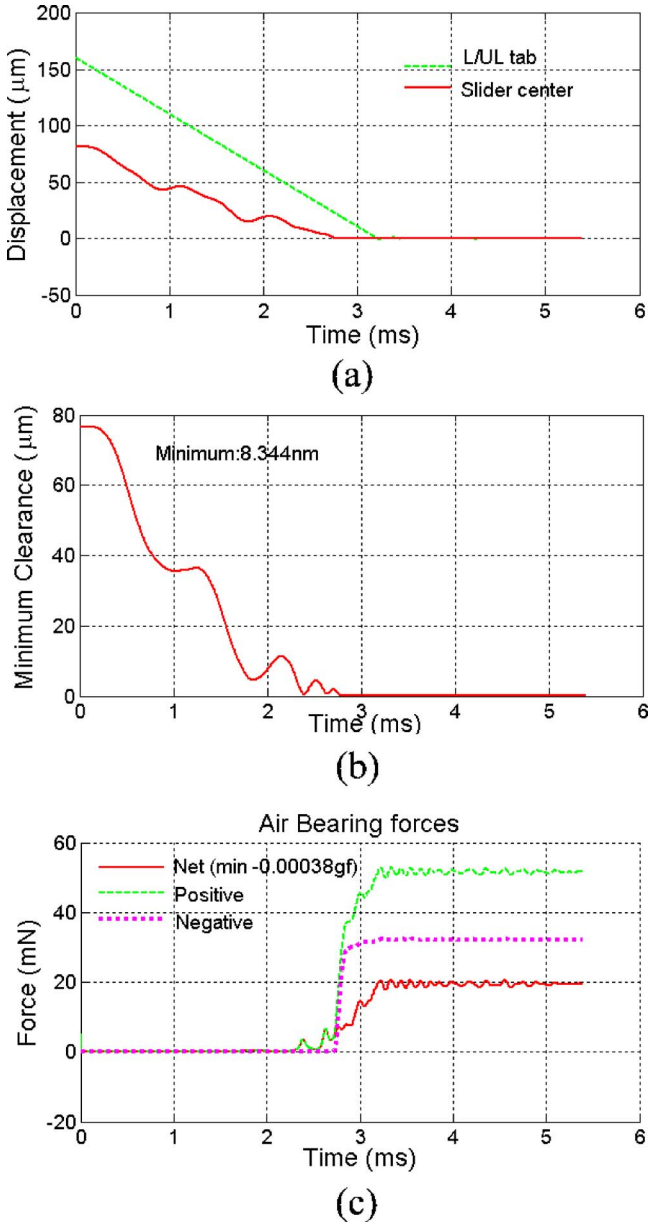


**Fig. 15 Displacement, minimum clearance and force histories during loading at the OD with 50 mm/s loading velocity and 15,000 rpm disk velocity**

other conventional ABS designs. The CML L/UL and shock simulator was used to investigate the L/UL of Slider B with a finite element model for the suspension. The simulator models actuator rotation over a prescribed ramp profile. The unloading process takes place at the OD (29.89 mm, 7.22 deg) and 15,000 rpm. The displacements and the minimum clearances during unloading at 50 mm/s and 150 mm/s are shown in Fig. 13(*a*). The minimum clearance drops due to the unloading process are illustrated in Fig. 13(*b*). It is seen that the minimum clearance drops merely 0.3 nm even at a high velocity. Figure 14 shows the air bearing forces during unload. The liftoff forces are−0.74 and −0.79 giga force (gf) at 50 mm/s and 150 mm/s, respectively. The displacement, minimum clearance and air bearing forces during the loading process are shown in Fig. 15. Similarly, there is no contact observed in the process.

**4.3 Flying Height Modulation.** In order to quantitatively compare the FHM of the ABS designs, we measured the topography of a current "super-smooth" disk surface by laser Doppler vibrometer (LDV) and used it as external excitation in the simulations. Figure 16 shows the measured disk morphology used in the simulations at three radial positions. The peak to peak and standard deviation ($\sigma$) of the disk roughness are 1.76 and 0.31 nm, respectively. Figure 17 shows a comparison of the FHMs of Slider B and Slider A. The quantitative results are summarized in Table 5, which includes peak to peak and standard deviation. The maximum peak-to-peak FHMs of Slider B and Slider A are found to be 0.36 nm (at the ID) and 0.47 nm (at the OD), respectively. Slider B exhibits a lower ratio of the maximum to minimum peak-to-peak value than Slider A. In cross-comparing ABS designs at different radial positions, Slider B is found to have 35–47% less FHM than Slider A at the MD and the OD but has 100% more FHM at the ID. The higher FHM of Slider B at the ID is due to the relatively higher skew (−15.62 deg) and the minute positive pressure under the central trailing pad. Such FHM can be further suppressed by the dynamic feedback controller proposed by Juang and Bogy [7,8].

## 5 Conclusion

This paper proposes a novel ABS design, Slider B, for a FH control slider with a piezoelectric nanoactuator, where the gap FH

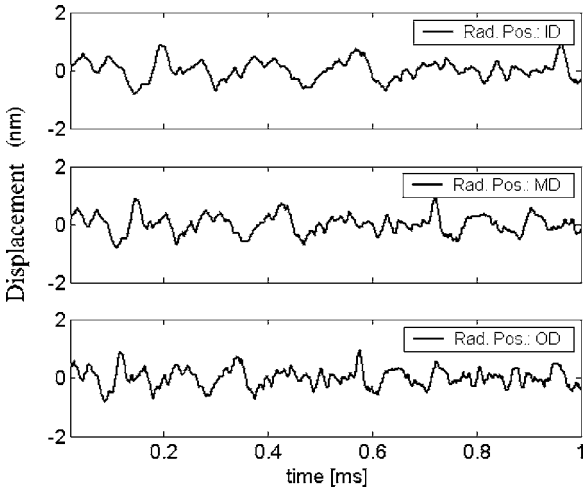


**Fig. 16 Measured disk morphology used in the simulation at three radial positions, ID, MD, and OD. The peak-to-peak and standard deviation of the disk roughness are 1.76 nm and 0.31 nm, respectively**

can be adjusted by applying an electrical voltage to the central piece of the piezoelectric material attached to the backside of the slider. Dynamic analysis shows that Slider B exhibits virtually 100% actuation efficiency, which indicates that the gap FH can be efficiently reduced by the actuator for ultrahigh density magnetic recording. A uniform FH and near-zero roll angle were achieved across the disk. The FH loss at a high altitude (4500 m) was found to be ~30%, which can be readily compensated for by the actuator with a pressure sensor. Slider B showed a significant increase in damping ratios and roll stiffness compared to several conventional designs, which was beneficial to better track-seeking and L/UL processes. The FH drop was reduced to ~0.2 nm during the track-seeking motion. Even though the Slider B has a considerable high negative force (−3.1 gf), the minimum clearance dropped merely 0.3 nm even at a high unloading velocity. The peak-to-peak FHM of Slider B simulated with a measured disk topography was found to be 0.17–0.36 nm. The higher value at the ID was due to the relative higher skew (−15.62 deg) and the minute positive pressure under the central trailing pad. Furthermore, the nanoscale adhesion forces, such as electrostatic and intermolecular forces, were found to be much less compared to conventional designs due to the fact that the FH control slider flies relatively higher with the miniature microtrailing pad in the close proximity of the disk surface, which greatly enhances the head/disk interface stability and reliability in ultrahigh density magnetic recording.

**Table 5 Simulations of FHM with actual measured disk topography for slider B and slider A**

| | Air bearing design | | |
|---|---|---|---|
| | Slider B | Slider A | Slider B/Slider A (%) |
| ID: peak to peak (nm) | 0.36 | 0.18 | 200 |
| ID: $\sigma$ (nm) | 0.06 | 0.03 | 200 |
| MD: peak to peak (nm) | 0.17 | 0.26 | 65.38 |
| MD: $\sigma$ (nm) | 0.02 | 0.04 | 50.00 |
| OD: peak to peak (nm) | 0.23 | 0.47 | 48.94 |
| OD: $\sigma$ (nm) | 0.03 | 0.07 | 42.86 |
| Max. $p$-$p$/min. $p$-$p$ | 212% | 261% | — |
| Max. $\sigma$/min. $\sigma$ | 300% | 233% | — |

## Acknowledgment

This study is supported by the Computer Mechanics Laboratory (CML) at the University of California, Berkeley and Information Storage Industry Consortium (INSIC). J. Y. Juang has also been supported by The California State Nanotechnology Fellowship.

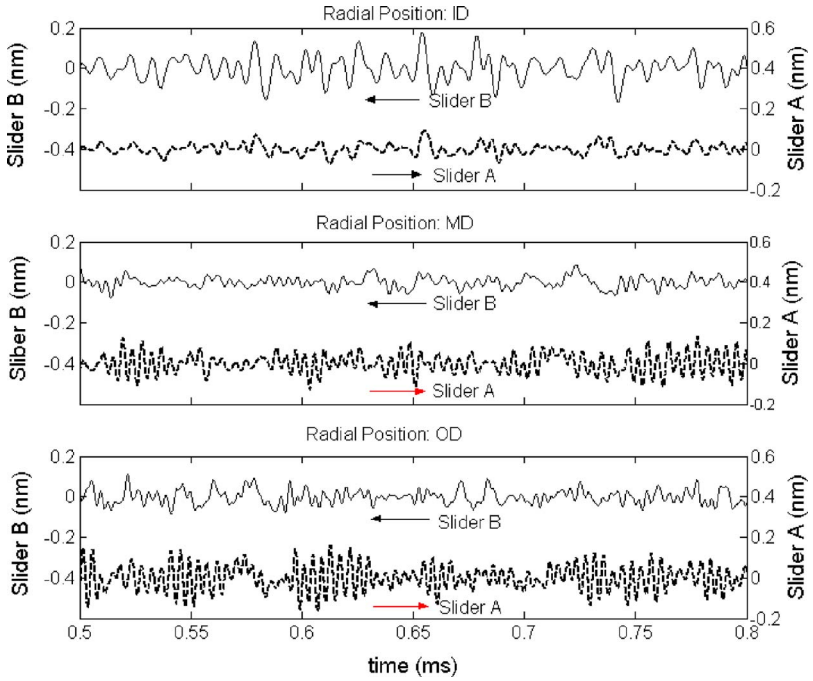


**Fig. 17 Comparison of FHMs of Slider B and Slider A at three radial positions, ID, MD, and OD with skews −15.62 deg, −2.56 deg, and 7.22 deg, respectively. The solid and dash curves are the results of Slider B and Slider A, respectively.**

## References


[1] Yanagisawa, M., Sato, A., Ajiki, K., and Watanabe, F., 1997, "Design Concept of Contact Slider for High-Density Recording," Electron. Commun. Jpn., Part 2: Electron., **80**(10), pp. 43–48.

[2] Kurita, M., Yamazaki, T., Kohira, H., Matsumoto, M., Tsuchiyama, R., Xu, J., Harada, T., Inoue, Y., Su, L., and Kato, K., 2002, "An Active-Head Slider with a Piezoelectric Actuator for Controlling Flying Height," IEEE Trans. Magn., **38**(5), pp. 2102–2104.

[3] Kurita, M., and Suzuki, K., 2004, "Flying-Height Adjustment Technologies of Magnetic Head Sliders," IEEE Trans. Magn., **40**(1), pp. 332–336.

[4] Suzuki, K., Maeda, R., Chu, J., Kato, T., and Kurita, M., 2003, "An Active Head Slider Using a Piezoelectric Cantilever for in situ Flying-Height Control," IEEE Trans. Magn., **39**(2), pp. 826–831.

[5] Tagawa, N., Kitamura, K.-I., and Mori, A., 2003, "Design and Fabrication of MEMS-Based Active Slider Using Double-Layered Composite PZT Thin Film in Hard Disk Drives," IEEE Trans. Magn., **39**(2), pp. 926–931.

[6] Su, L., Kurita, M., Xu, J., Kato, K., Adachi, K., and Miyake, Y., 2005, "Static and Dynamic Characteristics of Active-Head Sliders," Tribol. Int., **38**(6–7), pp. 717–723.

[7] Juang, J. Y., and Bogy, D. B., 2005, "Controlled-Flying Proximity Sliders for Head-Media Spacing Variation Suppression in Ultralow Flying Air Bearings," IEEE Trans. Magn., **41**(10), pp. 3052–3054.

[8] Juang, J. Y., and Bogy, D. B., 2006, "Nonlinear Compensator Design for Active Sliders to Suppress Head-Disk Spacing Modulation in Hard Disk Drive," IEEE/ASME Trans. Mechatron., 11(3), pp. 256–264.

[9] Yeack-Scranton, C. E., Khanna, V. D., Etzold, K. F., and Praino, A. P., 1990, "An Active Slider for Practical Contact Recording," IEEE Trans. Magn., **26**(5), pp. 2478–2483.

[10] Juang, J. Y., Bogy, D. B., and Bhatia, C. S., 2006, "Numerical and Experimental Study of an $Al_2O_3$-TiC Slider with a Piezoelectric Nanoactuator," *Proceedings of the ASME/JSME Joint Conference on Information and Precision Equipment (MIPE)*, Santa Clara, CA, June.

[11] Khanna, V. D., Hendriks, F., and Praino, A. P., 1991, "Programmable Air Bearing Sliders," IEEE Trans. Magn., **27**(6), pp. 5145–5147.

[12] Zhang, M., Yu, S., Liu, J., and Liu, B., 2005, "Flying Height Adjustment by Slider's Air Bearing Surface Profile Control," J. Appl. Phys., **97**(10), p. 10P309.

[13] Dietzel, A., Berger, R., Mächtle, P., Despont, M., Häberle, W., Stutz, R., Binnig, G. K., and Vettiger, P., 2002, "In Situ Slider-to-Disk Spacing on a Nanometer Scale Controlled by Microheater-Induced Slider Deformations," J. Am. Ceram. Soc., **100**(1), pp. 123–130.

[14] Meyer, D. W., Kupinski, P. E., and Liu, J. C., 1999, "Slider with Temperature Responsive Transducer Positioning," U. S. Patent No. 5,991,113, Nov. 23.

[15] Juang, J. Y., Chen, D., and Bogy, D. B., 2006, "Alternate Air Bearing Slider Designs for Areal Density of 1 Tbit/in.$^2$," IEEE Trans. Magn., **42**(2), pp. 241–246.

[16] Juang, J. Y., and Bogy, D. B., "Air Bearing Surface Design for Flying Height Control Sliders with Thermal Nanoactuator," unpublished.

[17] Chen, F., Xie, H., and Fedder, G. K., 2001, "Microactuator for Ultra-Low Magnetic Disk Head Fly Height Control," IEEE Trans. Magn., **37**(4), pp. 1915–1918.

[18] Song, D., Schnur, D., and Boutaghou, Z.-E., 2004, "Discharge Mechanism for Electrostatic Fly Control," IEEE Trans. Magn., **40**(4), pp. 3162–3164.

[19] Feng, Z., Shih, C. Y., Poon, C.-S. F., and Gubbi, V. K., 2003, "Method for Controlling Flying Height of a Magnetic Head," U.S. Patent No. 6,529,342B1, March 4.

[20] Albrecht, T. R., Fontana, R. E. Jr., Kasiraj, P., Klaassen, E. H., Payne, R. N., and Reiley, T. C., 2002, "Flying Height Adjustment for Air Bearing Sliders," U. S. Patent No. 6,344,949, Feb. 5.

[21] Good, D. L., Mason, J. E., and Ottesen, H. H., 1994, "Fly Height Servo Control of Read/Write Head Suspension," U.S. Patent No. 5,377,058, December 27.

[22] Liu, X., Li, A., Clegg, W., Jenkins, D. F. L., and Davey, P., 2002, "Head-Disk Spacing Variation Suppression via Active Flying Height Control," IEEE Trans. Instrum. Meas., **51**(5), pp. 897–901.

[23] Zeng, Q. H., and Bogy, D. B., 1999, "Stiffness and Damping Evaluation of Air Bearing Sliders and New Designs with High Damping," ASME J. Tribol., **121**(2), pp. 341–347.

[24] Thornton, B. H., and Bogy, D. B., 2004, "A numerical Study of Air-Bearing Slider Form-Factors," ASME J. Tribol., **126**(3), pp. 553–558.

[25] Boutaghou, Z.-E., Qian, W., Olim, M., Sannino, A., Zhu, J., and Serpe, C., 2005, "Disc Head Slider with Subambient Pressure Cavity Bottom Surfaces of Different Depths," U.S. Patent No. 6,934,122 B2, August 23.

[26] Gupta, V., and Bogy, D. B., 2005, "Dynamics of Sub-5-nm Air-Bearing Sliders in the Presence of Electrostatic and Intermolecular Forces at the Head Disk Interface," IEEE Trans. Magn., **41**(2), pp. 610–615.

[27] Bhargava, P., and Bogy, D. B., 2005, "Numerical Simulation of Load/Unload in Small Form Factor Hard Disk Drives," Computer Mechanics Lab., Department of Mechanical Engineering, University of California, Berkeley, Technical Report No. 2005-011.

[28] Zeng, Q. H., and Bogy, D. B., 1999, "Slider Air Bearing Designs for Load/Unload Applications," IEEE Trans. Magn., **35**(2), pp. 746–751.

[29] Bogy, D. B., and Zeng, Q. H., 2000, "Design and Operating Conditions for Reliable Load/Unload Systems," Tribol. Int., **33**(5–6), pp. 357–366.

[30] Suk, M., and Gillis, D., 1998, "Effect of Slider Burnish on Disk Damage During Dynamic Load/Unload," ASME J. Tribol., **120**(2), pp. 332–338.